Does fixed-interval sampling suffice for water distribution system monitoring? An adaptive strategy via time-frequency analysis

Shaosong Wei[1], Zhigang Liu[2], Jie Fei[3], Tingchao Yu[4], Avi Ostfeld[5], Shipeng Chu[6*]

Abstract: Sensors in water distribution systems (WDSs) generally use fixed-interval sampling, such as once every 15 minutes, but whether this sampling frequency meets actual monitoring and modeling needs, has not been sufficiently explored. This study continuously collected pressure monitoring data from three locations in a WDS at a 100Hz sampling frequency for one month. Frequency analysis reveals that the signal is non-stationary, with frequency characteristics varying significantly across different periods of the day. Since the information content (e.g., high-frequency details) conveyed by the signal differs across time, this necessitates time-varying sampling requirements to adequately capture critical data in each period. Based on these findings, an adaptive sampling method (ASM) for WDS monitoring is proposed. Experimental results demonstrate that the proposed ASM achieves a more uniform distribution of reconstruction error (i.e., the discrepancy between the original high-frequency signal and its reconstruction from sampled data) and a lower overall error magnitude, compared with the traditional fixed-interval sampling method (FISM). This study systematically investigates hydraulic data sampling in WDSs under pressure conditions unaffected by anomalous variations, such as sudden pipe bursts or extraordinary operational actions (e.g., valve maneuvers or atypical pump operations). The analysis is based on signal characteristics and provides a foundation for the design of intelligent monitoring networks in WDSs.

Keywords: Adaptive Sampling, Fast Fourier Transform, Short-Time Fourier Transform, Water Distribution System

[1] PhD student, College of Civil Engineering and Architecture, Zhejiang University, Hangzhou 310058, PR China. Email: shaosongwei@zju.edu.cn;

[2]Engineer, Ningbo Water and Environment Group Co., Ltd, Ningbo, CHINA, 315012. E-mail: zcigmondliu@126.com

[3]Engineer, Ningbo Water and Environment Group Co., Ltd, Ningbo, CHINA, 315012. E-mail: 1037644987@qq.com

[4]Professor, College of Civil Engineering and Architecture, Zhejiang University, Hangzhou 310058, PR China. Innovation Center of Yangtze River Delta, Zhejiang University, Jiaxing 314100, PR China. Zhejiang Key Laboratory of Intelligent Control for Urban Water Systems, Zhejiang University, Hangzhou 310058, PR China. Email: yutingchao@zju.edu.cn;

[5] Professor, Civil and Environmental Engineering, Technion - Israel Institute of Technology, Haifa ISRAEL. Email: ostfeld@cv.technion.ac.il

[6]Assistant Professor, College of Civil Engineering and Architecture, Zhejiang University, Hangzhou 310058, PR China (corresponding author). Email: chushipeng@zju.edu.cn

Practical Applications: This study updates the understanding of WDS hydraulic state dynamics, which supports core water utility tasks such as online simulation and real-time scheduling, and confirms WDS hydraulic states are dynamic, non-stationary processes rather than steady states that fixed-frequency sampling can fully capture. Conventional fixed-frequency monitoring lacks systematic verification of its ability to capture WDS dynamic changes, and has inherent flaws: it causes insufficient monitoring during high-variability periods, and generates redundant data during low-variability periods, leading to unnecessary resource waste. The proposed adaptive sampling method balances data accuracy and resource occupation; under the same sampling volume, it achieves more uniform sampling error distribution, higher overall monitoring accuracy, and complete capture of hydraulic changes that are easily overlooked by fixed-frequency sampling, providing a data-driven direction for efficient WDS monitoring.

Introduction

In recent years, intelligent technologies have been increasingly applied in WDSs, encompassing hydraulic models (Bartos et al. 2024), machine learning (Gross et al. 2025; Hao et al. 2022), and deep learning (Alvisi et al. 2025; Hao et al. 2024). These technologies, serving as proactive management tools, focus on addressing core issues in WDSs - such as state estimation (Rego et al. 2022), leakage detection (Daniel et al. 2022; Oberascher et al. 2024), and district metering (Xie et al. 2024) - with their effective implementation relying crucially on massive real-time monitoring data (Hu et al. 2023; Mahmoud et al. 2022; Zhang et al. 2023). Driven by this growing reliance on continuous monitoring, pressure and flow sensors have become widely deployed in WDSs. These sensors routinely transmit system measurements to the cloud at fixed intervals to support real-time analytics and operational decision-making. However, despite the widespread adoption of 5 - 15-minute sampling intervals in regions like the UK (Mounce et al. 2012) and China (Yu et al. 2022) for years, whether this fixed-interval sampling suffices for WDS monitoring has not been fully explored.

While higher sensor sampling frequencies enhance data precision, practical engineering constraints inherently limit their unrestricted increase. On the operational front, battery-powered sensors face proportional increases in power consumption and data storage costs with higher sampling rates, straining water utilities' maintenance budgets (Du et al. 2015). Technically, elevated sampling frequencies also overload hardware - software systems by escalating data collection and processing demands (Cominola et al. 2018). This creates a trade-off between balancing data precision and operational efficiency, a challenge that is central to intelligent monitoring network design and operation.

Against this backdrop, while fields like agriculture (Zhang et al. 2024) , ecology (Lehtiniemi et al. 2022), and hydrology (He et al. 2022) have systematically studied this relationship, WDSs remain underexplored. Existing research on WDSs has primarily focused on water demand sampling (Cominola et al. 2018; Heydari et al. 2022) and transient pressure sampling for burst detection (Mounce et al. 2012; Ye and Fenner 2014), as well as determining minimum sampling frequencies for transient event detection (Kim et al. 2024b). In contrast, pressure data in WDSs support a wide range of applications (Mounce et al. 2012; Ye and Fenner 2014), and the networks typically operate under pressure conditions not affected by anomalous variations for the majority of the time. The commonly adopted sampling interval of 5–15 minutes is based on assumptions corresponding to these stable conditions. However, this practice has historically lacked comprehensive empirical validation from a signal characteristics perspective.

The Nyquist - Shannon Sampling Theorem (Shannon 1949) dictates that reconstructing a continuous-time signal from discrete samples without aliasing requires the sampling frequency to be at least twice the signal's maximum frequency component-with a stricter standard recommending four times this value to capture wave crests and troughs adequately (Choi et al. 2015). In the context of WDSs, this theorem presents unique challenges because pressure signals exhibit pronounced dynamic characteristics driven by periodic variations as well as the superimposed effects of operational and failure events. These dynamics mean that WDS signals can have drastically different frequency profiles across days or even within the same day, as they are event related. Based on the sampling theorem (Shannon 1949), sampling frequency should adapt: reduced when signals have low frequencies to conserve power resources and increased during high-frequency events to maintain precision and thus enhance event detection such as leaks and transient occasions. Yet existing fixed-interval sampling methods (FISM; e.g., 5-minute intervals) overlook this temporal variability, failing to align with WDS signals' time-varying nature, thus instantly requiring the development of adaptive sensor sampling algorithms to meet changing monitoring requirements.

Adaptive sensor sampling strategies, by optimizing the number of sampling points across different time periods (i.e., sampling intervals), offer a promising solution to balance data precision and operational efficiency without increasing overall data volume. While such strategies have been applied in domains like agriculture (Rodriguez-Pabon et al. 2022) and greenhouse monitoring - where Kochhar et al. (2023) adjusted frequencies by comparing temporal data trends. However, WDS sensor signals differ fundamentally in two key aspects. First, they are driven by regular daily cycles in water demand, resulting in periodic fluctuations that are not commonly addressed in previous ASM studies (Hu et al. 2021; Huang et al. 2021; Ristow et al. 2021). Second, they are subjected to abrupt, high-impact disturbances (e.g., pump startups, pipe bursts, environmental noise), introducing non-stationary frequency components that far exceed the variability seen in, for instance, greenhouse humidity or soil moisture signals (Song et al. 2023; Wu et al. 2024; Zhang et al. 2024). This dual nature - periodic yet influenced by various operational disturbances and failure events - makes WDS signals unique. Unlike adaptive algorithms designed for environmental data, existing methods fail to account for WDS signals' time-varying frequency profiles and abrupt transient events. As the dynamic frequency characteristics of WDS remain understudied, there is an urgent need to develop adaptive sampling frameworks that explicitly adapt to both the daily periodicity and operational disturbances and failure events, ensuring optimal data quality while minimizing operational costs.

To address this gap in understanding how to optimize sampling frequency for WDS pressure data, particularly from the perspective of the signal's inherent time-varying characteristics, this study collected high-frequency pressure data from an operational WDS in a southern Chinese city. To address this unmet need, this study first characterized the signal's non-stationary frequency dynamics using Fast Fourier Transform (FFT) and Short-Time Fourier Transform (STFT) time-frequency analyses, revealing distinct daily periodicity and abrupt frequency shifts driven by real-world disturbances. These insights formed the basis for developing a stable ASM that adjusts intervals according to instantaneous frequency content. Analysis results show that, under the same data volume condition, the proposed strategy not only achieves higher data precision but also ensures a more uniform distribution of reconstruction errors, effectively balancing data quality and operational efficiency in WDS monitoring. This work represents a new systematic exploration of hydraulic data sampling in WDS from a signal-characteristics perspective, providing a foundation for intelligent monitoring networks in WDS.

2. Materials and Methodology

2.1 Data Collection

The high-frequency monitoring data used in this study were obtained from a large-scale, real-world WDS in China. The system is equipped with three pressure sensors, which are installed at different locations within the network: a main pipeline, a terminal node, and a regional pump station. The sensor sampling frequency was set to 100 Hz, which is the highest frequency used in previous studies (Choi et al. 2015; Kim et al. 2024a; b) to ensure the collected data closely capture actual pressure behavior, while maintaining a balance between data volume and accuracy. The monitoring data were collected over a 30-day period. Data for the terminal node spanned 22 days, owing to temporary equipment maintenance during the monitoring period. The sensor installation locations are shown in Figure 1, where the main pipeline is highlighted in red. Additionally, Figure 2 illustrates the pressure time series recorded over a 1-week period at the three sampling sites, complementing the spatial-temporal data presented in Figure 1.

2.2 Frequency Analysis of Pressure Data

To analyze the overall frequency distribution of the monitoring data, frequency-domain analysis was performed on the pressure data from the three sampling sites using the FFT. Additionally, the STFT was applied to analyze the periodic variations in the pressure signal frequencies and how they change at different times.

2.2.1 Fast Fourier Transform（FFT）

The Fourier Transform is a widely used signal processing tool that converts time-domain signals into their frequency-domain representations, thereby revealing the spectral characteristics of the signal. However, the traditional Discrete Fourier Transform has a high computational complexity of $O(N^2)$, which makes it impractical for large-scale data analysis. To overcome this, the FFT algorithm, which reduces the computational complexity to $O(N\ log\ N)$, was employed in this study, significantly improving computational efficiency.

In this work, FFT was applied to perform frequency-domain analysis on the collected pressure data to identify the primary frequency components. Given a discrete signal $\boldsymbol{x}(n)$ of length N, the FFT is defined as:

$$\boldsymbol{m}(f) = FFT(p_1, p_2, \cdots, p_N) \tag{1}$$

where, $\boldsymbol{m}(f)$ represents the energy associated with different frequency f; $FFT(\cdot)$ denotes the Fast Fourier Transform; and $p_1, p_2, \cdots, p_N$ refer to the pressure data used in the transformation, with N being the total number of pressure data points.

FFT enables efficient global spectral analysis of the pressure signal, ignoring temporal frequency variations to enhance computational efficiency and frequency resolution. By transforming the pressure signal from the time domain to the frequency domain, FFT reveals the constituent frequency components and their energy distribution, thereby providing a theoretical basis for determining an appropriate sampling frequency for pressure monitoring in WDSs.

2.2.2 Short-Time Fourier Transform (STFT)

While FFT is effective at revealing the overall frequency distribution of a signal, it assumes that the signal is stationary over the entire time domain (i.e., its statistical properties do not change over time). However, real-world signals are often non-stationary, with their spectral characteristics varying over time. To address this, the STFT was applied for time-frequency analysis.

The STFT segments the signal using a sliding window function, such that each segment can be treated as stationary. FFT is then applied to each windowed segment to obtain spectral information that varies over time. The STFT is defined as:

$$\boldsymbol{m}(f, t) = STFT(p_1, p_2, \ldots, p_N) \tag{2}$$

where, $\boldsymbol{m}(f,t)$ represents the signal energy at frequency f within the time window centered at t; $STFT(\cdot)$ denotes the Short-Time Fourier Transform. After applying the transformation, the energy distribution across different frequencies can be obtained for each time window. In this study, a Hanning window was specifically employed to reduce spectral leakage. Optimized window length and overlap ratio were chosen using the grid search algorithm to achieve better time and frequency resolution. The computed time-frequency spectrograms were used to analyze the signal's frequency characteristics across time, illuminating its dynamic properties.

As a valuable complement to the FFT, the STFT divides the original pressure signal into multiple short time windows and performs an FFT on each segment, thereby capturing the time-varying frequency content of the signal. By capturing time-varying frequency features, this process provides a scientific basis for developing more effective and rational sampling strategies, thereby bridging the gap between signal characteristics and adaptive sampling design. This method enables the identification of non-stationary characteristics in pressure data, making it particularly suitable for analyzing dynamic behaviors in WDSs.

2.3 Adaptive Sampling Strategy Design

2.3.1 Adaptive Sampling interval optimization

In current engineering practice, the most commonly used FISM assumes that the signal remains stationary throughout the data collection process. However, in practical applications, the pressure monitoring data exhibit significant non-stationarity, with the energy distribution of frequency components varying over time. Based on the STFT analysis, an ASM was proposed, in which the sampling frequency is dynamically adjusted according to the energy of the frequency components in different time periods. This approach enhances the ability to capture critical variations in the pressure signal while improving the efficiency and accuracy of data acquisition.

After obtaining the energy distribution across time and frequency using Eq. (2), the energy of the pressure signal is first normalized along the frequency dimension.

$$\widehat{\boldsymbol{m}}(f,t) = \frac{\boldsymbol{m}(f,t) - min_t\{[\boldsymbol{m}(f,t)]\}}{max_t\{[\boldsymbol{m}(f,t)]\} - min_t\{[\boldsymbol{m}(f,t)]\}} \tag{3}$$

where, $\widehat{\boldsymbol{m}}(f,t)$ represents the normalized energy distribution of different frequency f within the time window centered at t; $max_t\{[\boldsymbol{m}(f,t)]\}$ and $min_t\{[\boldsymbol{m}(f,t)]\}$ are the maximum and minimum energy for all time window.

At each time window, for mitigating the influence of high-frequency noise in the pressure signal, a low-pass filter is applied to remove the spectral energy components above the cutoff frequency:

$$\ddot{\boldsymbol{m}}(f,t) = \hat{\boldsymbol{m}}(f,t), f \leq f_c \tag{4}$$

where, f_c is the cutoff frequency, and $\ddot{\boldsymbol{m}}(f,t)$ represents the truncated energy distribution.

Furthermore, the mean of the truncated energy distribution along the frequency dimension is first calculated.

$$\bar{\boldsymbol{m}}(t) = \frac{\sum_{f=0}^{f_c} \ddot{\boldsymbol{m}}(f,t)}{n} \tag{5}$$

where, $\bar{\boldsymbol{m}}(t)$ is the mean of the truncated energy distribution along the frequency dimension, and n is the total number of frequency components.

Then, for each time window, the variance of the energy distribution across different frequency components can be calculated as follows:

$$var(t) = \frac{\sum_{f=0}^{f_c} [\ddot{\boldsymbol{m}}(f,t) - \bar{\boldsymbol{m}}(f,t)]^2}{n-1} \tag{6}$$

where, $var(t)$ is the variance of the energy distribution across different frequency components.

By using $var(t)$ as the weighting factor for sample allocation, the number of samples assigned to each time window can be calculated:

$$s_t = M \frac{[var(t)]^\gamma}{\sum_{t=0}^{T} [var(t)]^\gamma} \tag{7}$$

where, s_t is the number of samples allocated to the time window centered at t; M is the predefined total number of samples per day; and γ is the exponent parameter of the variance, used to adjust the importance of the variance in the allocation process.

The proposed sampling strategy consists of three main components. The first component involves performing time-frequency analysis on daily pressure data using the STFT. The second component calculates the variance of the energy for each sliding window. The third component assigns different numbers of sampling points to each window based on the variance of the energy. The rationale behind this proposed strategy is that the pressure in WDSs primarily occupies lower-frequency regions. When the sliding window moves into periods dominated by low-frequency signals, the variance in energy is small, leading to fewer sampling points, which are sufficient for capturing the low-frequency signals. Conversely, when the window encompasses periods with both

low - and high-frequency signal distributions, the variance in energy increases, resulting in more sampling points to adequately capture the higher-frequency signals.

2.3.2 Moving Average Sampling

To mitigate the inevitable noise impact on single-sample data, a Moving Average Sampling (MAS) strategy is adopted. This approach involves collecting m consecutive samples at a fixed interval (e.g., 0.01s between each sample) and computing their mean as the representative value for that sampling period:

$$\breve{y}_i = \sum_{j=i-k}^{i+k} y_j \tag{8}$$

where, $\breve{y}_i$ is the sampled value at time step i , and the parameter $2k + 1$, representing the number of consecutive samples, which is optimized to balance noise reduction and data efficiency. By leveraging the statistical property that random noise tends to cancel out in averaged values, MAS effectively attenuates high-frequency disturbances while preserving the underlying signal trend. By adjusting m based on real-time noise levels or signal characteristics (e.g., using grid search or adaptive algorithms), the strategy can dynamically optimize the trade-off between noise suppression and sampling overhead, making it suitable for diverse monitoring scenarios in WDSs or other sensor networks.

2.4 Sampling Simulation and Evaluation

In the sampling evaluation, the data for both FISM and ASM were generated by subsampling the high-frequency (100 Hz) pressure data. If the sampled values were compared with the original high-frequency data only at the sampling instants (i.e., direct sampling), the resulting error would always be zero, which fails to reflect the actual performance of the algorithms. Therefore, to robustly evaluate the proposed ASM, an assessment method was developed to overcome the limitation of direct sampling. The approach involves:

1) Sampling data from the original 100 Hz signal using the algorithm to simulate real-world sensor sampling.

2) Reconstructing 100 Hz data via interpolation between sampling points, as direct sampling alone cannot evaluate accuracy.

3) Applying a moving average filter (MAF) to the original noisy data, then using residual magnitude and distribution uniformity between reconstructed and filtered data as evaluation metrics.

The mean absolute error (MAE) between the reconstructed and filtered data as evaluation metrics. The MAE is calculated as:

$$MAE = \frac{1}{N}\sum_{i=1}^{N}|y_i - \hat{y}_i| \quad (9)$$

where N is the number of samples, y_i is the true value of the i-th sample, and $\hat{y}_i$ is the predicted value for the i-th sample. The absolute difference $|y_i - \hat{y}_i|$ represents the error between the true and predicted values for each sample.

Beyond absolute error, the temporal uniformity of reconstruction errors is selected as another metric. This is achieved by computing the standard deviation of the MAE for each hour using the following formulation:

$$STD = \sqrt{\frac{\sum_{i=1}^{N}\{|y_i - \hat{y}_i| - MAE\}^2}{N-1}} \quad (10)$$

3. Results and Analysis

3.1 Frequency Content Analysis

3.1.1 Frequency Domain Analysis

Figure 2 shows the pressure time series recorded at the three monitoring sites. Overall, the pressures at all sites fluctuate within a relatively stable range. The mean pressures at Sensor #1, Sensor #2, and Sensor #3 are approximately 29.9 m, 30.3 m, and 41 m, respectively, each displaying clear periodic variations. The diurnal patterns at Sensors #1 and #2 are mainly driven by daily water-demand cycles, whereas the periodicity at Site #3 is associated with scheduled pump operations. All three datasets also exhibit random fluctuations and occasional outliers, indicating the presence of measurement noise—a well-recognized issue in pressure data acquisition (Mounce et al. 2012; Shao et al. 2024; Zhao et al. 2017).

FFT was applied to examine the pressure data in the frequency domain. Figure 3 shows the FFT results for the three sampling sites. The signal energy is mainly concentrated in the low-frequency band, whereas the high-frequency components contain only minor energy. This indicates that pressure dynamics are dominated by low-frequency variations, consistent with the fact that pressure changes in WDSs are largely driven by daily water-demand cycles.

According to Choi et al. (2015), the sampling frequency should be at least four times the highest significant frequency component to ensure accurate signal representation. Accordingly, Figure 3 marks the maximum frequency detectable under a 10-minute sampling interval using red dashed lines. The spectral results

show that most high-energy components of the pressure signal lie within this detectable range, suggesting that the commonly used 10-minute interval is generally sufficient for characterizing steady-state behavior in WDSs. However, this assessment assumes that the pressure signal is fully stationary. From an average perspective, the 10-minute interval appears appropriate, but the inherent non-stationarity of pressure data implies that the actual required sampling frequency may be considerably higher. Therefore, in practice, the sampling rate should be adaptively adjusted to account for the signal's non-stationary characteristics, ensuring a more accurate reflection of system dynamics.

3.1.2 Time-Frequency Domain Analysis

To further examine the time–frequency characteristics of the pressure data, the STFT was applied to the measurements from the three sampling sites. The window length plays a critical role in shaping the time–frequency representation: longer windows provide better frequency resolution but smooth short-term variations, whereas shorter windows improve temporal resolution while diminishing the ability to distinguish low-frequency components. Given that pressure signals in WDSs are dominated by low-frequency dynamics, excessively short windows may obscure these dominant features, while overly long windows may suppress meaningful high-frequency fluctuations.

To balance these trade-offs and capture frequency dynamics across multiple temporal scales, three window lengths were selected. The 2-day window enables analysis of inter-day frequency variations, the 2-hour window provides a balanced resolution suitable for characterizing intra-day dynamics, and the 20-minute window offers finer temporal detail while preserving sufficient low-frequency resolution. Together, these windows support a comprehensive assessment of the time-varying frequency characteristics of the pressure signals.

Figures 4a–4c present the STFT results for the three sampling sites using a 2-day window with a 1-day overlap. As the sliding window progresses along the time axis, the energy distribution across frequencies varies, demonstrating that the pressure data are not stationary. The dominant frequency components at all three sites remain concentrated in the low-frequency range, consistent with the FFT results.

Figures 4d–4f show the STFT results for the three sampling sites using a 2-hour window with a 1-hour overlap. For each site, the STFT was first applied to the daily pressure data, and the resulting energy values were then averaged. The results indicate that all three sites exhibit pronounced high-frequency components during specific periods of the day, while low-frequency components dominate the remaining periods. At the terminal and main-pipe sites, notable high-frequency activity occurs between 5:00–8:00 am, 4:00–5:00 pm, and 11:00–

12:00 pm. At the pump station, high-frequency components are most prominent from 6:00–11:00 am. These temporal patterns show that the pressure signals undergo significant fluctuations at certain times of the day but remain relatively stable during others, highlighting the non-stationary nature of the data—contrary to the stationarity assumed in the FFT analysis.

Similar to Figures 4d–4f, Figures 4g–4i present the STFT results for the three sampling sites using a 20-minute window with a 10-minute overlap. Comparing Figures 4g–4i with Figures 4d–4f shows that longer windows capture more low-frequency components, whereas shorter windows highlight higher-frequency variations. Thus, the choice of window length substantially influences the STFT results. Nevertheless, this variation does not change the main conclusion: the pressure data in the WDS are inherently non-stationary, exhibiting pronounced high-frequency components during certain periods and predominantly low-frequency components during others.

The time–frequency analysis shows that periods with elevated high-frequency energy correspond to a greater need for higher sampling frequencies. For the terminal and main pipeline sites, stronger high-frequency components occur between 5:00–8:00, 16:00–17:00, and 23:00–24:00. At the pump station, this occurs between 6:00–11:00. In contrast, during periods with lower high-frequency energy, the required sampling frequency is correspondingly reduced.

To quantify the sampling requirements over time, the variance of spectral energy within each time window was used as an indicator. Higher variance indicates stronger high-frequency fluctuations and thus a greater sampling demand, while lower variance reflects energy concentrated in the low-frequency range and a reduced sampling need. Figure 5 presents the spectral energy variance across 2-hour windows with 50% overlap for Sensor #1, Sensor #2, and Sensor #3, using cutoff frequencies of 0.28, 0.6, and 0.88, respectively. With the 50% overlap, the effective time resolution is 1 hour.

As illustrated by the comparison of Figures 4 and 5, the spectral energy variance effectively captures temporal variations in sampling requirements. In Figure 5(a), the variance is notably high between 5:00 and 8:00 each day, indicating the need for increased sampling frequency during this period. Consistently, Figure 4(d) shows a more dispersed energy distribution over the same interval, demonstrating that the variance-based metric reliably reflects the non-stationary behavior of pressure data in the WDS. Building on this insight, an ASM is proposed, where the number of samples allocated to each period is determined according to the quantified demand derived from spectral energy variance.

3.2 Adaptive Sampling

Previous studies have generally assumed that pressure sensors in WDSs follow a FISM, implicitly presuming that system pressure remains completely stable over time (Chu et al. 2021; Santos-Fernandez et al. 2024; Zhou et al. 2023). However, the analysis in the previous section demonstrates that this assumption is invalid. Consequently, applying a uniform sampling frequency throughout the day leads to under-sampling during periods with high-frequency activity and over-sampling when low-frequency components dominate, resulting in uneven information capture. This unevenness is evident in the reconstruction errors when low-frequency sampled data are used to reconstruct the underlying true signal, showing variable error distributions across the day. To address this issue, an ASM was developed based on the variance of spectral energy within sliding time–frequency windows. Windows with higher variance are assigned more sampling points, whereas those with lower variance receive fewer samples (Eq. (7)).

3.2.1 High-frequency Data Denoising

In this study, a MAF was applied to the high-frequency (100 Hz) pressure data to remove noise and estimate the underlying true signal. This filtered signal was used as the reference baseline for assessing the performance of different sampling strategies. The MAF window length was optimized through a systematic trial-and-error process over a range of 20, 40, 60, 80, 100, and 120 s, with a final value of 1 min selected to balance effective high-frequency noise reduction and the preservation of meaningful signal dynamics.

Figure 6 compares the raw and denoised pressure signals recorded over three consecutive days at the three sampling sites. The denoised signals exhibit smoother profiles, more accurately reflecting the true variations in system pressure. In contrast, the high-frequency fluctuations around the filtered signal in the raw data represent stochastic disturbances within the system, which are effectively removed by the denoising process.

3.2.2 Accuracy of Reconstruction Data

In the proposed ASM, the parameter γ in Eq. (7) controls the influence of spectral energy variance on sample allocation. Larger γ values increase the weight of variance, whereas smaller values reduce it. Based on a systematic evaluation of γ = 1, 2, and 3 using the objective function STD defined in Eq. (10), the optimal γ was determined to be 1 for Sensor #1 and Sensor #2, and 2 for Sensor #3. In addition, the window length significantly affects the time–frequency energy distribution, which in turn shapes the variance across time periods: longer windows emphasize low-frequency components, while shorter windows highlight high-frequency variations. To reduce the influence of high-frequency noise, frequencies above the designated cutoff were excluded when

computing variance, ensuring that the variance distribution more accurately reflects the actual situation. Optimal window lengths and cutoff frequencies under different sampling conditions were determined using a grid optimization algorithm, with the objective function STD defined in Eq. (10). The resulting optimized parameters are summarized in Tables S1 and S2, which are provided in the Supporting Information.

Figure 7b presents the reconstruction error histograms for each hourly period when 288 samples are collected (i.e., FISM interval of 5 minutes) at Sensor #1, comparing the FISM strategy with the proposed ASM. The ASM markedly reduces overall reconstruction errors compared to FISM, with the MAE decreasing from 0.1128 to 0.0746. This improvement stems from the ASM's ability to optimize the sampling distribution by allocating points according to the varying demands of different periods. For example, during the 7th hourly time window, the pressure signal contains more high-frequency components, and FISM produces large errors. In contrast, the 21st hourly time window is dominated by low-frequency components, resulting in smaller errors under FISM. The ASM addresses this by assigning more samples to high-demand periods like the 7th hourly time window and fewer to low-demand periods like the 21st hourly time window, thereby improving overall sampling efficiency. Reconstruction errors under different sites and sampling quantities are summarized in Table 1 and Figures S1–S21, with the latter provided in the Supporting Information, which are consistent with this analysis.

Figures 7a and 7c show the reconstruction error histograms for each hourly period when 960 and 48 samples are collected (i.e., FISM intervals of 1.5 minutes and 30 minutes) at Sensor #1, comparing the FISM approach with the proposed ASM. As before, applying the ASM substantially reduces reconstruction errors. However, the improvement becomes less pronounced at lower sampling rates. This is because reduced sampling increases interpolation errors, which limits the relative information gain achieved through optimized sample allocation.

3.2.3 Error Uniformity of Reconstruction Data

Regarding error uniformity, Figure 7b shows that the ASM markedly improves the uniformity of pressure reconstruction errors at all three sampling sites compared to the FISM approach. For Sensor #1, the uniformity metric STD decreased from 0.0344 under FISM to 0.0149 with ASM. This improvement arises from the ASM's refined allocation of sample points: windows with stronger high-frequency components are assigned more samples, while those with weaker high-frequency content receive fewer samples. Reconstruction error uniformity across different sites and sampling quantities is summarized in Table 1 and Figures S1–S21 in the Supporting

Information. These results align with the preceding analysis, further demonstrating the robustness and generalizability of the proposed ASM.

As shown in Figures 7a and 7c, the ASM improves the uniformity of pressure reconstruction errors across different sample quantities. When 960 samples are used, the uniformity metric STD decreases from 0.0248 under FISM to 0.0059 with ASM. For 48 samples, STD decreases from 0.0533 to 0.0401. Figure 7 demonstrates similar trends across different sampling quantities. However, as the number of samples decreases, the improvement in uniformity becomes less pronounced. This is primarily because fewer samples limit the number of points that can be allocated to each window, reducing the refinement of the adaptive sampling process. As a result, subtle variations in the pressure signal's frequency are harder to capture, leading to smaller performance gains with ASM. However, this limitation is reasonable, as achieving highly refined sample allocation with very few samples is inherently challenging.

Discussion

This study addressed the critical question of whether FISM suffices for WDS pressure monitoring, and proposed ASM grounded in time-frequency analysis. The core outcome— that ASM outperforms FISM in reducing overall reconstruction error and improving error uniformity— stems from its ability to align sampling frequency with the non-stationary nature of WDS pressure signals. Unlike FISM, which assumes signal stationarity and leads to under-sampling during high-variability periods and over-sampling in low-variability phases, ASM dynamically allocates sampling points based on spectral energy variance (Eq.(6)), ensuring critical high-frequency details are captured without redundant data. This alignment with the Nyquist-Shannon Sampling Theorem addresses the long-standing trade-off between data precision and operational efficiency in WDS monitoring, providing a data-driven solution for intelligent sensor network design.

Beyond the primary performance gains, the study's time-frequency analysis (FFT and STFT) offers deeper insights into WDS hydraulic dynamics: pressure signals are dominated by low-frequency components driven by daily water demand cycles, yet exhibit pronounced high-frequency fluctuations during specific time windows (e.g., 5:00–8:00 am). This finding challenges the implicit assumption of steady-state pressure in conventional monitoring, emphasizing that sampling strategies must account for temporal variability to avoid information loss. However, the proposed ASM has inherent methodological limitations: using spectral energy variance as the sampling allocation metric may occasionally misreflect high-frequency component proportions— significant variance can arise even in predominantly low-frequency signals, potentially wasting sampling

resources. While setting a cutoff frequency to partition high- and low-frequency bands is a conceptual solution, noise-induced spectral distortion complicates optimal cutoff determination, limiting generalizability. Additionally, the reliance on basic FFT and STFT, while practical for implementation, may insufficiently capture extreme non-stationarity or transient events; advanced techniques like wavelet analysis or semblance analysis could enhance resolution for complex WDS environments.

The findings are derived from 30-day high-frequency data (22 days for one sensor) collected from three locations in a single WDS, and spectral characteristics of pressure signals may vary across different WDS types, geographical settings, or seasons. While the observed sampling demand trends are generalizable, ASM parameters (e.g., window length, γ) must be tailored to specific deployment contexts. Practically, this requires short-term high-frequency pre-sampling (e.g., 100 Hz) to characterize site-specific signal dynamics, a step that ensures adaptability but adds initial setup overhead.

Although the ASM demonstrates clear advantages, its applicability may not be universal in certain scenarios. For example, ASM may not be suitable for water balance analysis. In water distribution network districts with multiple inlets and outlets, applying ASM to flow data could result in temporally misaligned signals, thereby hindering accurate estimation of net inflow. Similarly, the analysis of pressure fluctuations induced by demand variations requires temporal alignment between pressure and flow-rate signals. The development of more flexible adaptive sampling strategies to accommodate diverse data application scenarios will be explored in future work.

Conclusions

For a long time, FISM has been used in WDSs sensor sampling. To assess whether this fixed interval is sufficient to capture the essential monitoring information and to better reflect the distribution of information within the data, this study investigates the required sampling frequency for pressure monitoring in WDSs and proposes an ASM. The objective is to identify a more appropriate sampling frequency and strategy for WDS monitoring in order to more accurately enhance the effectiveness of information acquisition and ensure the reliable operation of water infrastructure. Based on the analysis and the proposed ASM, the following key findings and practical implications are summarized:

(1) Through frequency domain analysis using the FFT, it was found that the widely adopted 10-minute sampling interval captures most pressure data information on average based on the assumption that the pressure signal behaves as a stationary time series.

(2) In practice, the pressure signal in WDSs is non-stationary. STFT analysis reveals that the pressure signal exhibits varying frequency characteristics across different periods of the day, resulting in time-varying sampling requirements. Certain periods exhibit higher energy in the high-frequency components, indicating a greater need for dense sampling, whereas other periods have lower sampling demands.

(3) Considering the non-stationary nature of pressure signals, this study proposed an ASM that accounts for the time-varying sampling demand by quantifying the energy variance of different frequency components derived from the STFT. The results show that, compared with the traditional FISM, the proposed strategy achieves more uniform sampling error distribution and lower overall error magnitude.

The limitations of the present study are that the above findings are based on high-frequency pressure data collected from three sensors in a single WDS, and the applicability and specific parameters of the ASM require tailored settings based on specific scenarios. Future research should address these limitations by: 1) validating the ASM across diverse WDSs (e.g., urban vs. rural, small vs. large-scale) and seasonal conditions to optimize parameter adaptability; 2) integrating advanced time-frequency analysis techniques to refine the sampling allocation metric, balancing accuracy and operational feasibility; 3) exploring the integration of the ASM with real-time noise reduction algorithms to mitigate the impacts of spectral distortion. 4) developing more flexible adaptive sampling strategies to accommodate a wide range of complex data application scenarios. By addressing these gaps, the adaptive sampling framework can be further refined to support more robust and cost-effective WDS monitoring, advancing the development of intelligent water infrastructure management systems.

Data availability Statement

Data will be made available on request.

Acknowledgments

This work was supported by Ningbo Science and Technology Plan Project (2023Z057), National Natural Science Foundation of China (Grant 52200119), the National Key Research and Development Program of China (2023YFC3208102, 2022YFF0606905), and by the Israeli Water Authority under project number 2033800.

Conflict of Interest

The authors declare that they have no known competing financial interests or personal relationships that could have appeared to influence the work reported in this paper.

References

Alvisi, *S*., M. Franchini, V. Marsili, F. Mazzoni, E. Salomons, M. Housh, A. Abokifa, K. Arsova, F. Ayyash, H. Bae, R. Barreira, L. Basto, S. Bayer, E. Z. Berglund, D. Biondi, F. Boloukasli Ahmadgourabi, B. Brentan, J. Caetano, F. Campos, H. Cao, S. Cardona, E. P. Carreño Alvarado, N. Carriço, G.-A. Chatzistefanou, Y. Coy, E. Creaco, S. Cuomo, A. de Klerk, A. Di Nardo, M. DiCarlo, U. Dittmer, R. Dziedzic, A. Ebrahim Bakhshipour, D. Eliades, R. Farmani, B. Ferreira, A. Gabriele, M. M. Gamboa-Medina, F. Gao, J. Gao, R. Gargano, M. Geranmehr, C. Giudicianni, K. Glynis, S. Gómez, L. González, M. Groß, H. Guo, M. N. Habibi, A. Haghighi, B. Hammer, L. Hans, M. Hayslep, Y. He, L. Hermes, M. Herrera, F. Hinder, B. Hou, A. Iglesias-Rey, P. L. Iglesias-Rey, I.-S. Jang, J. Izquierdo, M. S. Jahangir, C. Jara-Arriagada, B. Jenks, G. Johnen, M. Kalami Heris, M. Kalumba, M.-S. Kang, M. Khashei Varnamkhasti, K.-J. Kim, J. Kley-Holsteg, T. Ko, A. Koochali, P. Kossieris, P. Koundouri, C. Kühnert, A. Kulaczkowski, J. Lee, K. Li, Y. Li, H. Liu, Y. Liu, C. A. López-Hojas, A. Maier, C. Makropoulos, F. J. Martínez-Solano, N. H. Marzouny, A. Menapace, C. Michalopoulos, G. Moraitis, H. Mousa, H. Namdari, D. Nikolopoulos, M. Oberascher, A. Ostfeld, M. Pagano, F. Pasha, J. Perafán, G. Perelman, J. Pesantez, M. Polycarpou, M. G. Quarta, Q. Que, J. Quilty, C. Quintiliani, A. Ramachandran, G. Reynoso Meza, V. Rodriguez, Y. Romano, J. Saldarriaga, A. K. Salem, P. Samartzis, G. F. Santonastaso, D. Savic, V. Schiano Di Cola, D. Schol, A. G. Seyoum, R. Shen, K. Simukonda, A. Sinske, R. Sitzenfrei, B. Sonnenschein, I. Stoianov, A. Tabares, E. Todini, L. Tsiami, I. Tsoukalas, A.-J. Ulusoy, L. Vamvakeridou-Lyroudia, A. van Heerden, J. Vaquet, V. Vaquet, S. Wallner, M. Walraad, D. Wang, S. Wu, W. Wu, A. Wunsch, Y. Yao, J. Yu, A. Zanfei, D. Zanutto, H. Zhang, M. Ziebarth, F. Ziel, and J. Zou. 2025. “Battle of Water Demand Forecasting.” *Journal of Water Resources Planning and Management*, 151 (10): 04025049. American Society of Civil Engineers. https://doi.org/10.1061/JWRMD5.WRENG-6887.

Bartos, M., M. Thomas, M.-G. Kim, M. Frankel, and L. Sela. 2024. “Online state estimation in water distribution systems via Extended Kalman Filtering.” *Water Research*, 264: 122201. https://doi.org/10.1016/j.watres.2024.122201.

Choi, D. Y., J. Kim, D.-J. Lee, and D. Kim. 2015. “Pressure measurements with valve-induced transient flow in water pipelines.” *Urban Water Journal*, 12 (3): 200–206. IAHR Website. https://doi.org/10.1080/1573062X.2013.832778.

Chu, S., T. Zhang, T. Yu, Q. J. Wang, and Y. Shao. 2021. “A noise adaptive approach for nodal water demand estimation in water distribution systems.” *Water Research*, 192: 116837. https://doi.org/10.1016/j.watres.2021.116837.

Cominola, A., M. Giuliani, A. Castelletti, D. E. Rosenberg, and A. M. Abdallah. 2018. “Implications of data sampling resolution on water use simulation, end-use disaggregation, and demand management.” *Environmental Modelling & Software*, 102: 199–212. https://doi.org/10.1016/j.envsoft.2017.11.022.

Daniel, I., J. Pesantez, S. Letzgus, M. A. Khaksar Fasaee, F. Alghamdi, E. Berglund, G. Mahinthakumar, and A. Cominola. 2022. “A Sequential Pressure-Based Algorithm for Data-Driven Leakage Identification and Model-Based Localization in Water Distribution Networks.” *Journal of Water Resources Planning and Management*, 148 (6): 04022025. American Society of Civil Engineers. https://doi.org/10.1061/(ASCE)WR.1943-5452.0001535.

Du, R., L. Gkatzikisz, C. Fischione, and M. Xiao. 2015. “Energy efficient monitoring of water distribution networks via compressive sensing.” In: *2015 IEEE International Conference on Communications (ICC)*, 6681–6686.

Gross, M.-P., R. Taormina, and A. Cominola. 2025. “A Machine Learning-based framework and open-source software for Non Intrusive Water Monitoring.” *Environmental Modelling & Software*, 183: 106247. https://doi.org/10.1016/j.envsoft.2024.106247.

Hao, W., A. Cominola, and A. Castelletti. 2022. “Comparing Predictive Machine Learning Models for Short- and Long-Term Urban Water Demand Forecasting in Milan, Italy.” *IFAC-PapersOnLine*, 2nd IFAC Workshop on Control Methods for Water Resource Systems CMWRS 2022, 55 (33): 92–98. https://doi.org/10.1016/j.ifacol.2022.11.015.

Hao, W., A. Cominola, and A. Castelletti. 2024. “Combining wavelet-enhanced feature selection and deep learning techniques for multi-step forecasting of urban water demand.” *Environmental Research: Infrastructure and Sustainability*, 4 (3): 035005. IOP Publishing. https://doi.org/10.1088/2634-4505/ad5e1d.

He, Y., D. Hou, H. Huang, and J. Luo. 2022. “On the ideal groundwater sampling window by utilizing transition pumping period.” *Journal of Hydrology*, 610: 127796. https://doi.org/10.1016/j.jhydrol.2022.127796.

Heydari, Z., A. Cominola, and A. S. Stillwell. 2022. “Is smart water meter temporal resolution a limiting factor to residential water end-use classification? A quantitative experimental analysis.” *Environmental Research: Infrastructure and Sustainability*, 2 (4): 045004. IOP Publishing. https://doi.org/10.1088/2634-4505/ac8a6b.

Hu, S., J. Gao, D. Zhong, L. Deng, C. Ou, and P. Xin. 2021. “An Innovative Hourly Water Demand Forecasting Preprocessing Framework with Local Outlier Correction and Adaptive Decomposition Techniques.” *Water*, 13 (5): 582. Multidisciplinary Digital Publishing Institute. https://doi.org/10.3390/w13050582.

Hu, S., J. Gao, D. Zhong, R. Wu, and L. Liu. 2023. “Real-Time Scheduling of Pumps in Water Distribution Systems Based on Exploration-Enhanced Deep Reinforcement Learning.” *Systems*, 11 (2): 56. Multidisciplinary Digital Publishing Institute. https://doi.org/10.3390/systems11020056.

Huang, H., Z. Zhang, and S. Fengxuan. 2021. “An Ensemble-Learning-Based Method for Short-Term Water Demand Forecasting.” *Water Resources Management*, 35 (6): 1757–1773. Springer Nature B.V. https://doi.org/10.1007/s11269-021-02808-4.

Kim, H., K. J. Jung, S. Lee, and E. H. Jeong. 2024a. “Rapid response to pressure variations in water distribution networks through machine learning-enhanced data acquisition.” *AQUA - Water Infrastructure, Ecosystems and Society*, 73 (7): 1358–1371. https://doi.org/10.2166/aqua.2024.030.

Kim, H., S. Lee, E. Jeong, D. Kim, H. Kim, and K. Y. Hwang. 2024b. “Determining effective sampling frequencies for transient pressure events in water distribution systems optimal sampling for WDS transients.” *Flow Measurement and Instrumentation*, 98: 102650. https://doi.org/10.1016/j.flowmeasinst.2024.102650.

Kochhar, A., N. Kumar, and S. Aneja. 2023. “Variance adaptive sporadic sampling for greenhouse monitoring.” *Sustainable Computing: Informatics and Systems*, 37: 100825. https://doi.org/10.1016/j.suscom.2022.100825.

Lehtiniemi, M., E. Fileman, H. Hällfors, H. Kuosa, S. Lehtinen, I. Lips, O. Setälä, S. Suikkanen, J. Tuimala, and C. Widdicombe. 2022. “Optimising sampling frequency for monitoring heterotrophic protists in a

marine ecosystem." *ICES Journal of Marine Science*, 79 (3): 925–936. https://doi.org/10.1093/icesjms/fsab132.

Mahmoud, H., W. Wu, and M. M. Gaber. 2022. "A Time-Series Self-Supervised Learning Approach to Detection of Cyber-physical Attacks in Water Distribution Systems." *Energies*, 15 (3): 914. Multidisciplinary Digital Publishing Institute. https://doi.org/10.3390/en15030914.

Mounce, S. R., R. B. Mounce, and J. B. Boxall. 2012. "Identifying Sampling Interval for Event Detection in Water Distribution Networks." *Journal of Water Resources Planning and Management*, 138 (2): 187–191. American Society of Civil Engineers. https://doi.org/10.1061/(ASCE)WR.1943-5452.0000170.

Oberascher, M., C. Maussner, A. Cominola, and R. Sitzenfrei. 2024. "Sensitivity of model-based leakage localisation in water distribution networks to water demand sampling rates and spatio-temporal data gaps." *Journal of Hydroinformatics*, 26 (8): 1824–1837. https://doi.org/10.2166/hydro.2024.245.

Rego, B. S., S. G. Vrachimis, M. M. Polycarpou, G. V. Raffo, and D. M. Raimondo. 2022. "State Estimation and Leakage Detection in Water Distribution Networks Using Constrained Zonotopes." *IEEE Transactions on Control Systems Technology*, 30 (5): 1920–1933. https://doi.org/10.1109/TCST.2021.3130534.

Ristow, D. C. M., E. Henning, A. Kalbusch, and C. E. Petersen. 2021. "Models for forecasting water demand using time series analysis: a case study in Southern Brazil." *Journal of Water, Sanitation and Hygiene for Development*, 11 (2): 231–240. https://doi.org/10.2166/washdev.2021.208.

Rodriguez-Pabon, C., G. Riva, C. Zerbini, J. Ruiz-Rosero, G. Ramirez-Gonzalez, and J. C. Corrales. 2022. "An Adaptive Sampling Period Approach for Management of IoT Energy Consumption: Case Study Approach." *Sensors*, 22 (4). MDPI AG. https://doi.org/10.3390/s22041472.

Santos-Fernandez, E., J. M. Ver Hoef, E. E. Peterson, J. McGree, C. A. Villa, C. Leigh, R. Turner, C. Roberts, and K. Mengersen. 2024. "Unsupervised Anomaly Detection in Spatio-Temporal Stream Network Sensor Data." *Water Resources Research*, 60 (11): e2023WR035707. https://doi.org/10.1029/2023WR035707.

Shannon, C. E. 1949. "Communication in the Presence of Noise." *Proceedings of the IRE*, 37 (1): 10–21. https://doi.org/10.1109/JRPROC.1949.232969.

Shao, Y., C. Xu, T. Zhang, H. Shentu, and S. Chu. 2024. "Noise Removal for the Steady-State Pressure Measurements Based on Domain Knowledge of Water Distribution Systems." *Journal of Water*

573 *Resources Planning and Management,* 150 (3): 04023082. American Society of Civil Engineers.
574 https://doi.org/10.1061/JWRMD5.WRENG-6240.
575 Song, W., H. Yan, F. Li, T. Tao, H. Duan, K. Xin, and S. Li. 2023. "Development of Smoothed Particle
576 Hydrodynamics based water hammer model for water distribution systems." *Engineering Applications*
577 *of Computational Fluid Mechanics,* 17 (1): 2171139. Taylor & Francis.
578 https://doi.org/10.1080/19942060.2023.2171139.
579 Wu, S., J. Wang, H. Xu, S. Zhao, and J. Xu. 2024. "CritiCoder: An End-to-End Uncertain Regression Network
580 for Robust Macroscopic Pressure Models in Water Distribution Systems." *IEEE Transactions on*
581 *Computational Social Systems,* 11 (2): 2222–2233. https://doi.org/10.1109/TCSS.2023.3272330.
582 Xie, C., Z. Tian, J. Wang, T. Chen, and Z. Zhang. 2024. "Dynamic DMA Design Methodology Based on
583 Multilevel DMA and Multiobjective Optimization." *Journal of Water Resources Planning and*
584 *Management,* 150 (11): 04024047. American Society of Civil Engineers.
585 https://doi.org/10.1061/JWRMD5.WRENG-6515.
586 Ye, G., and R. A. Fenner. 2014. "Study of Burst Alarming and Data Sampling Frequency in Water Distribution
587 Networks." *Journal of Water Resources Planning and Management,* 140 (6): 06014001. American
588 Society of Civil Engineers. https://doi.org/10.1061/(ASCE)WR.1943-5452.0000394.
589 Yu, T., B. Lin, Z. Long, Y. Shao, I. E. Lima Neto, and S. Chu. 2022. "Asynchronous sensor networks for Nodal
590 water demand estimation in water distribution systems based on sensor grouping analysis." *Journal of*
591 *Cleaner Production,* 365: 132676. https://doi.org/10.1016/j.jclepro.2022.132676.
592 Zhang, M., W. Zhao, C. Zhu, and J. Li. 2024. "Influence of the sampling time interval of canopy temperature
593 on the dynamic zoning of variable rate irrigation." *Agricultural Water Management,* 295: 108754.
594 https://doi.org/10.1016/j.agwat.2024.108754.
595 Zhang, Q., J. Yang, W. Zhang, M. Kumar, J. Liu, J. Liu, and X. Li. 2023. "Deep fuzzy mapping nonparametric
596 model for real-time demand estimation in water distribution systems: A new perspective." *Water*
597 *Research,* 241: 120145. https://doi.org/10.1016/j.watres.2023.120145.
598 Zhao, J., W. Chen, K. Chevil, J. Been, G. V. Boven, S. Keane, and R. Kania. 2017. "Effect of Pressure
599 Sampling Methods on Pipeline Integrity Analysis." *Journal of Pipeline Systems Engineering and*
600 *Practice,* 8 (4): 04017016. American Society of Civil Engineers.
601 https://doi.org/10.1061/(ASCE)PS.1949-1204.0000273.

602 Zhou, X., J. Zhang, S. Guo, S. Liu, and K. Xin. 2023. “A convenient and stable graph-based pressure
603 estimation methodology for water distribution networks: Development and field validation.” *Water*
604 *Research*, 233: 119747. https://doi.org/10.1016/j.watres.2023.119747.
605

Table 1. Reconstruction error metrics of FISM and ASM under different sampling quantities for three sensors.

Sensor	Metric	Method	Sampling quantities							
			960	480	288	192	144	96	72	48
Sensor #1	MAE	FISM	0.083	0.095	0.113	0.123	0.129	0.138	0.141	0.153
		ASM	0.029	0.053	0.075	0.086	0.097	0.108	0.114	0.125
	STD	FISM	0.025	0.028	0.034	0.038	0.046	0.047	0.049	0.053
		ASM	0.006	0.011	0.015	0.022	0.028	0.029	0.034	0.040
Sensor #2	MAE	FISM	0.062	0.074	0.088	0.097	0.100	0.110	0.115	0.124
		ASM	0.025	0.047	0.066	0.075	0.083	0.093	0.098	0.109
	STD	FISM	0.013	0.016	0.021	0.026	0.029	0.034	0.039	0.044
		ASM	0.004	0.008	0.012	0.015	0.021	0.024	0.028	0.033
Sensor #3	MAE	FISM	0.170	0.187	0.206	0.218	0.222	0.239	0.244	0.267
		ASM	0.038	0.072	0.097	0.114	0.128	0.145	0.154	0.169
	STD	FISM	0.033	0.044	0.054	0.063	0.068	0.079	0.087	0.103
		ASM	0.014	0.029	0.040	0.050	0.057	0.069	0.076	0.095

Figure 1

Click here to access/download;Figure;Fig 1.tif

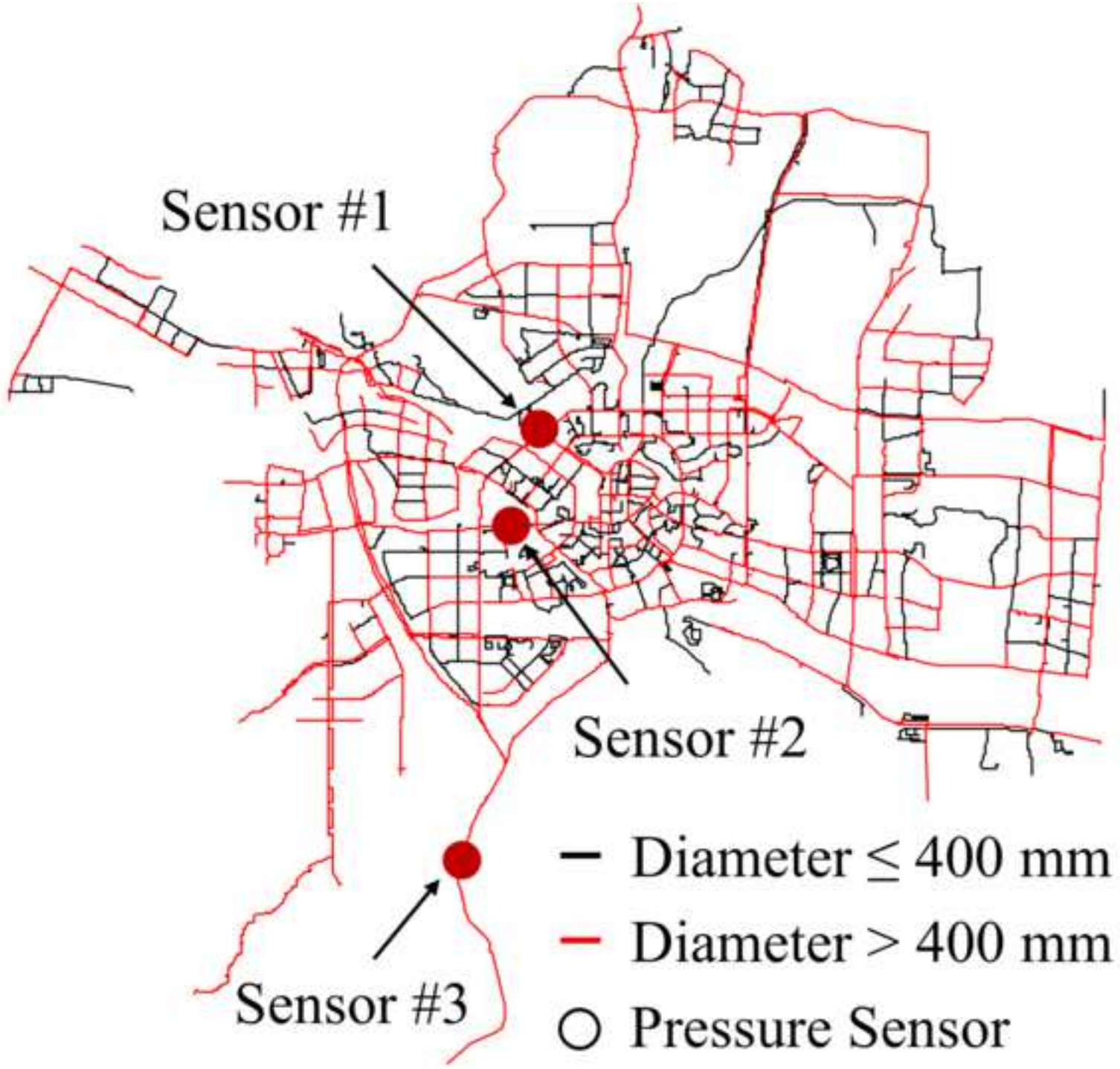

Figure 2

Click here to access/download;Figure;Fig 2.tif

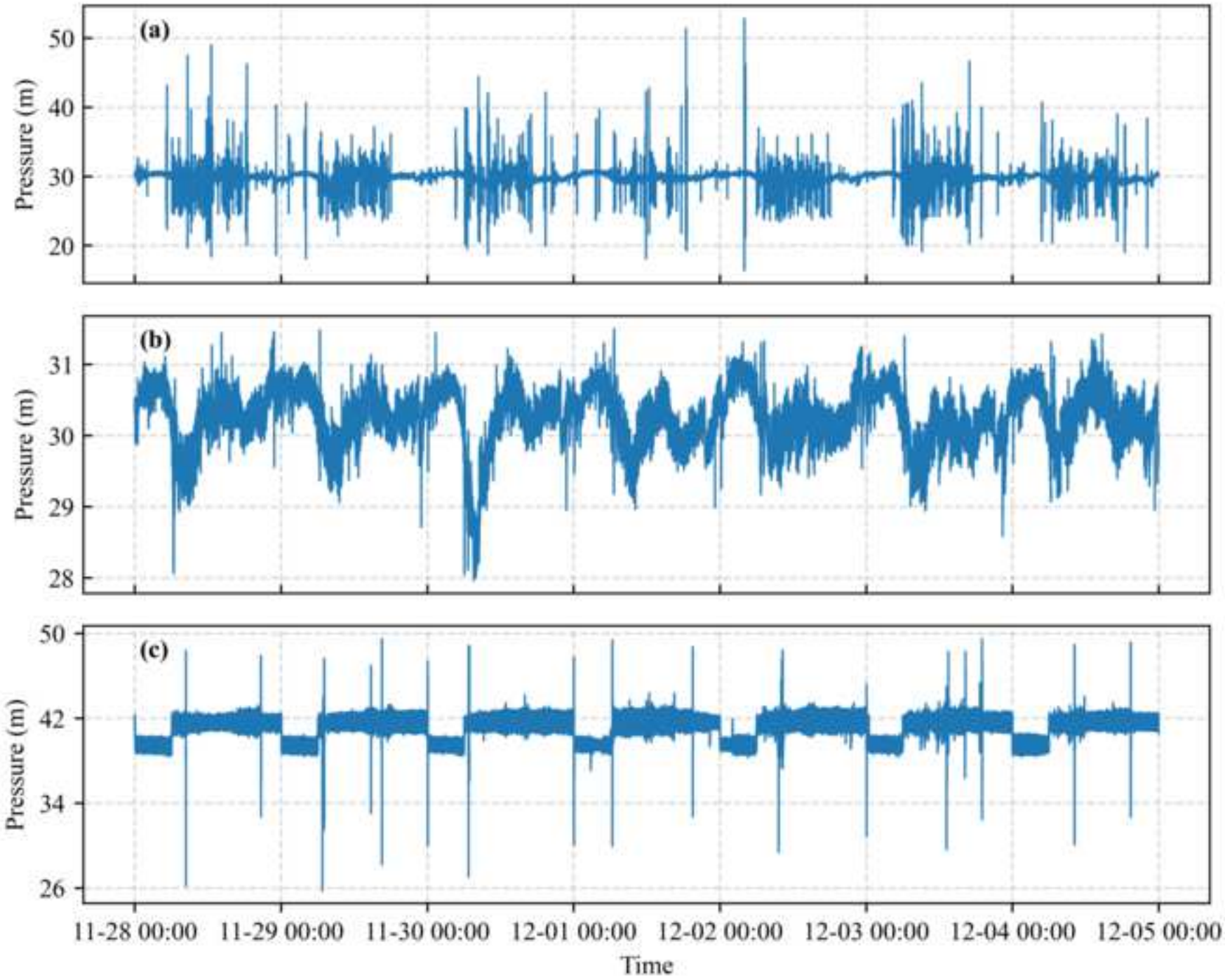

Figure 3

Click here to access/download;Figure;Fig 3.tif

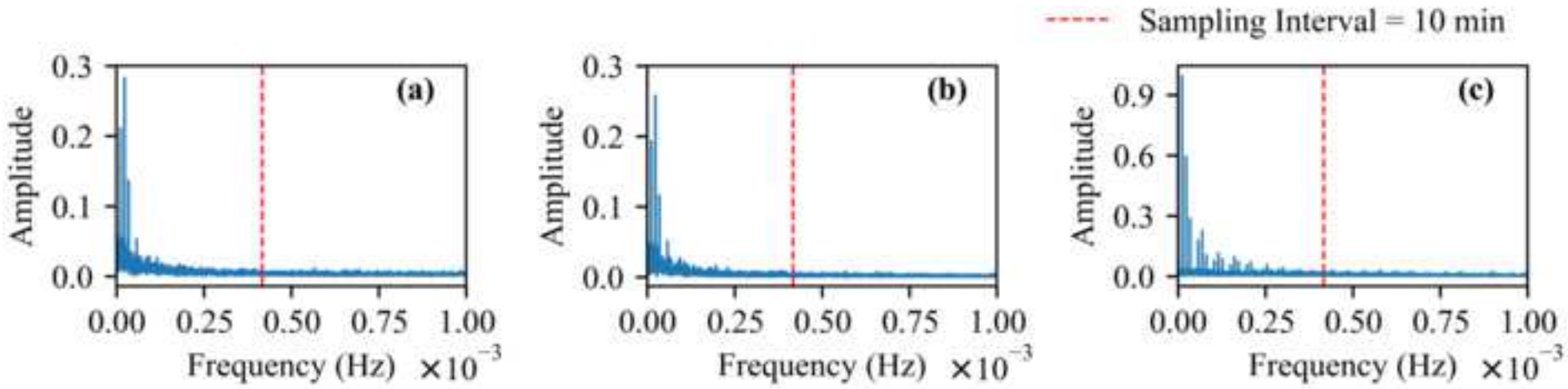

Figure 4

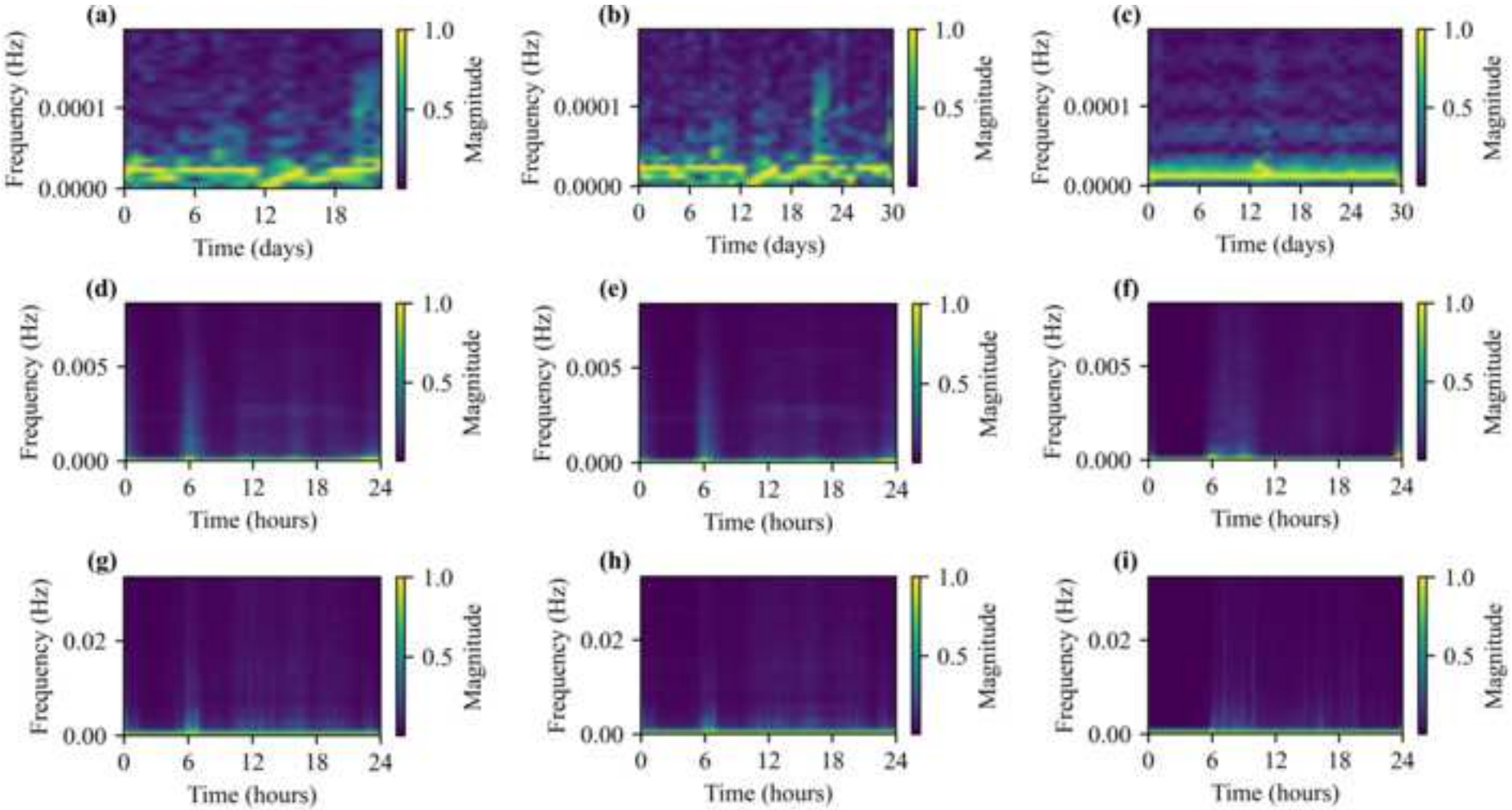

Figure 5

Click here to access/download;Figure;Fig 5.tif

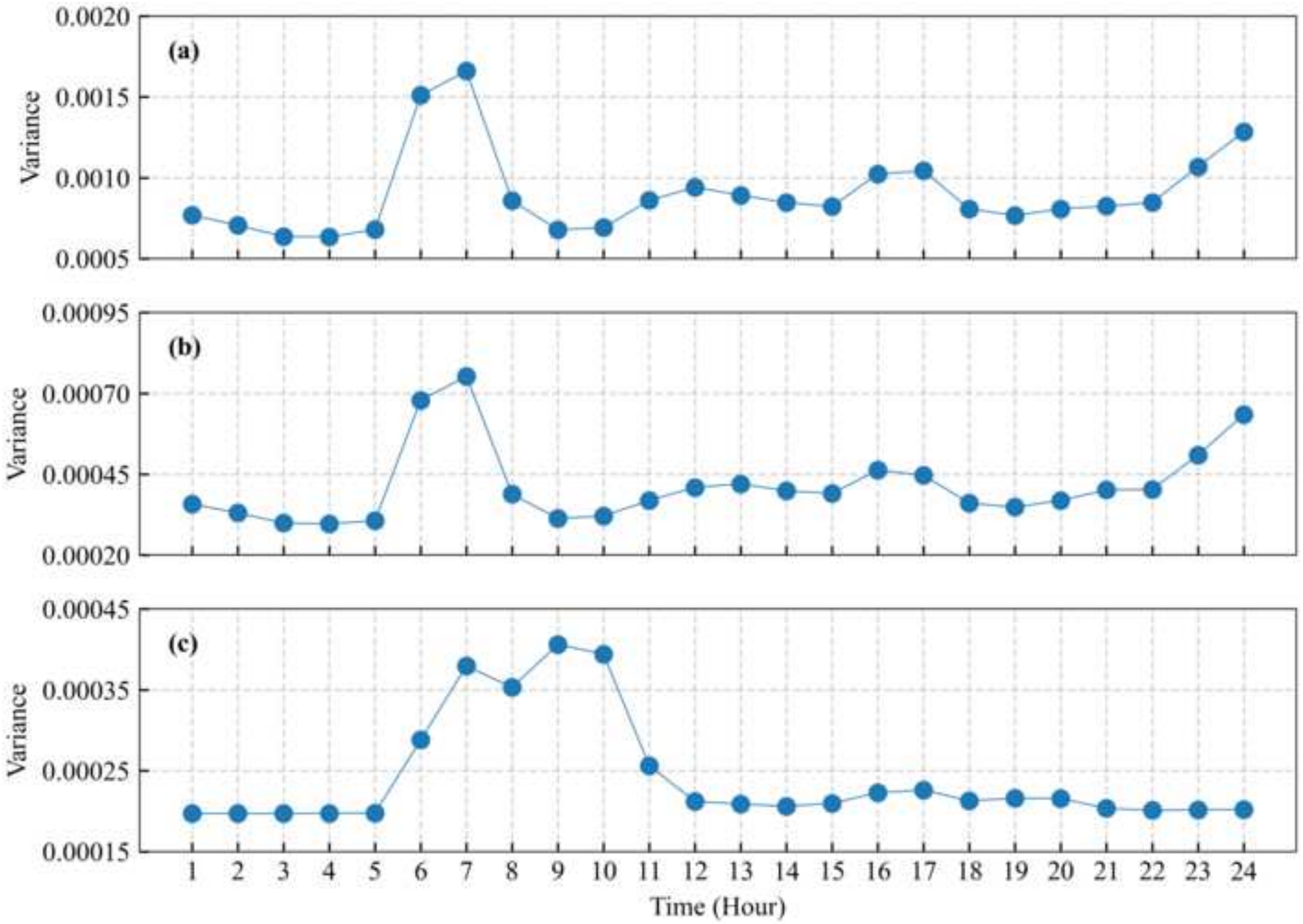

Figure 6

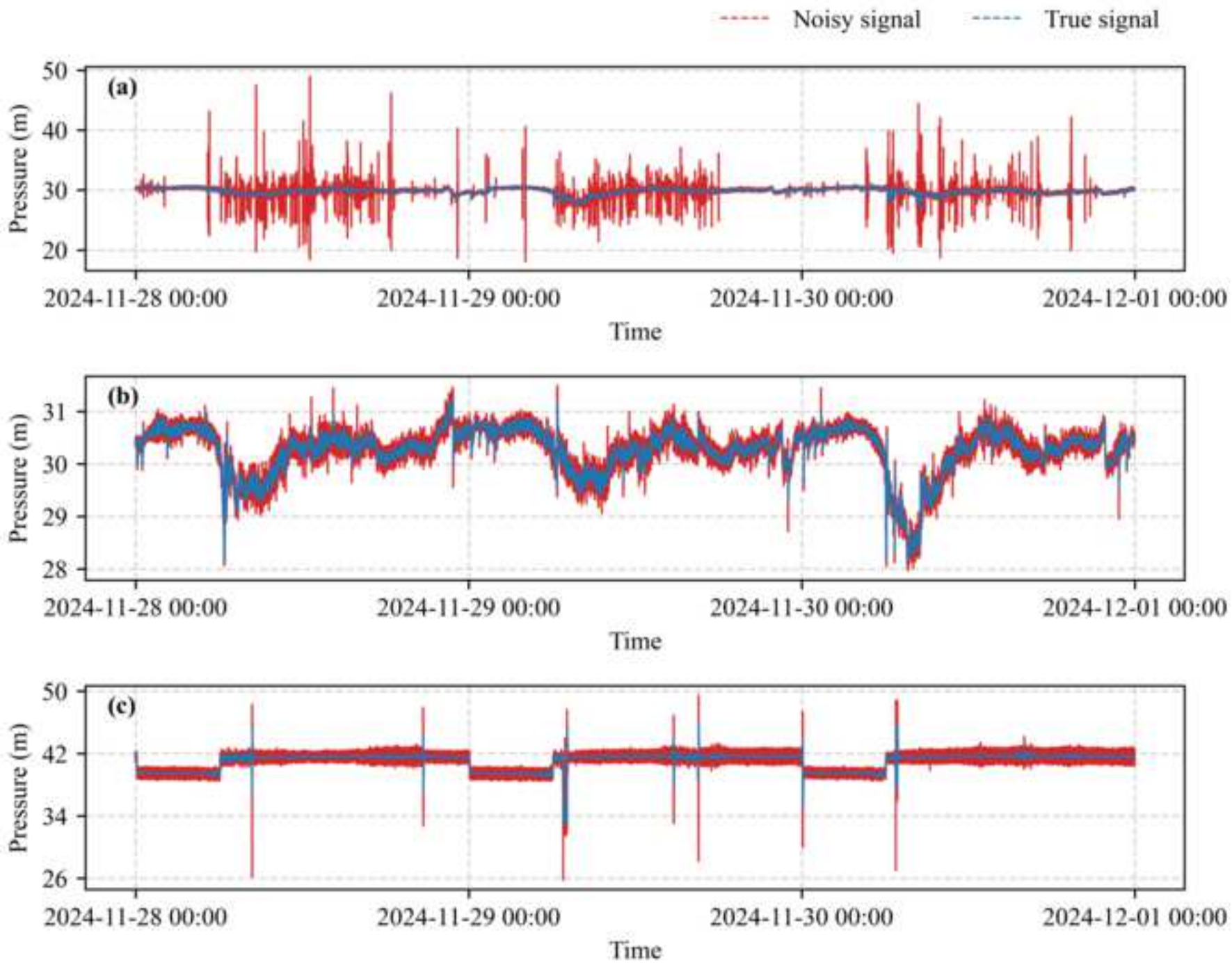

Figure 7

Click here to access/download;Figure;Fig 7.tif

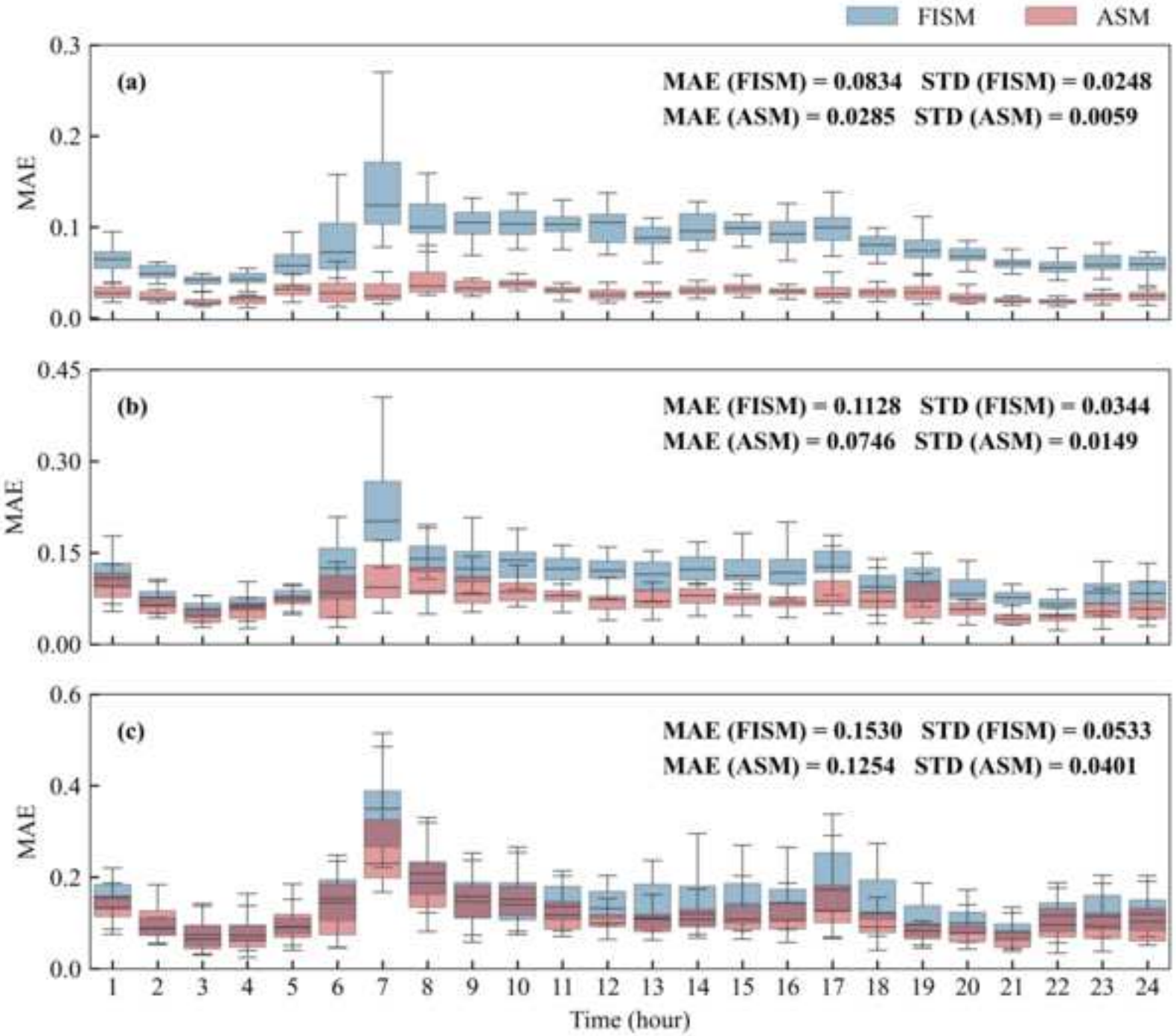

Fig. 1. Sensor installation locations, with red pipes denoting pipelines larger than 400 mm in diameter.

Fig. 2. Pressure time series for a 1-week period recorded at three sampling sites: (a) Sensor #1; (b) Sensor #2; (c) Sensor #3.

Fig. 3. FFT analysis results of pressure data recorded at three sampling sites: (a) Sensor #1; (b) Sensor #2; (c) Sensor #3.

Fig. 4. Time–frequency spectrograms of three sampling sites under different window lengths: (a) Sensor #1, 2 days; (b) Sensor #2, 2 days; (c) Sensor #3, 2 days; (d) Sensor #1, 2 hours; (e) Sensor #2, 2 hours; (f) Sensor #3, 2 hours; (g) Sensor #1, 20 minutes; (h) Sensor #2, 20 minutes; (i) Sensor #3, 20 minutes.

Fig. 5. Distribution of spectral energy variance across different time windows: (a) Sensor #1; (b) Sensor #2; (c) Sensor #3.

Fig. 6. Noisy signals and estimated true signals at the three sampling sites: (a) Sensor #1; (b) Sensor #2; (c) Sensor #3.

Fig. 7. Comparison of reconstruction error distributions after applying FISM and ASM at Sensor #1: (a) 960 samples; (b) 288 samples; (c) 48 samples.